DOI 10.1515/zkri-2013-1639 — Z. Kristallogr. 2014; 229(2): 101–111

Natsiri Satthaphut, Oliver B. Sutcliffe and Iain D. H. Oswald*

Putting the squeeze on mephedrone hydrogen sulfate

Abstract: Herein we report the characterisation of a novel salt of the *"legal high"* (±)-4′-methylmethcathinone hydrogen sulfate and its polymorphism under ambient and high pressure conditions. Under ambient pressure only one polymorph of the title compound was isolated but when subjected to high pressure a further two polymorphs are observed. The phase transitions at >0.5 GPa and >3.6 GPa are reversible single crystal to single crystal transitions which is possible due to the similarity of the packing in the molecules. It is proposed that these transitions are driven by the pV term of the Gibbs Free Energy equation rather than by the relief of repulsive interactions between molecules.

Keywords: high pressure, illicit materials, polymorphism, single-crystal transition

***Corresponding Author: Iain D. H. Oswald,** Strathclyde Institute of Pharmacy and Biomedical Sciences (SIPBS), University of Strathclyde, 161 Cathedral Street, Glasgow G4 0RE, UK, e-mail: iain.oswald@strath.ac.uk
For supplementary material see online version.
Natsiri Satthaphut: Strathclyde Institute of Pharmacy and Biomedical Sciences (SIPBS), University of Strathclyde, 161 Cathedral Street, Glasgow G4 0RE, UK
Oliver B. Sutcliffe: School of Science and the Environment, Manchester Metropolitan University, Chester Street, Manchester M1 5GD, UK

Introduction

Polymorphism in molecular materials is a well-documented phenonmenon potentially causing changes in the physicochemical properties of the materials in question [1, 2]. General methods for the exploration of the polymorphic behaviour of materals under ambient pressure include solvent screens [3, 4], heteronucleation on polymer surfaces [5, 8], and the alteration of the temperature [9–11] that the material is exposed to. In recent years, pressure has been increasingly used to study polymorphism of molecular materials, including amino acids [12–15], energetic materials [16–19], pharmaceuticals [20, 21], simple alcohols [22–24], and ionic liquids [25].

One class of compound that has not been explored in any great detail are illicit drugs [26, 27]. Due to their molecular structure, i.e. many functional groups and comformational flexibility, these materials have a significant potential for polymorphism. Like pharmaceutical products, the solid-state structure of these materials may affect the bioavailability and hence cause irreproducible doses of the active form to the body causing potential overdoses.

Recently, there has been a trend within the clubbing scene to make and distribute *"legal highs"* and hence there has been a striking increase in their sales [28]. These chemicals may be bought through the Internet at low cost and are sometimes pure compounds which display highly similar chemical structures to existing controlled substances within the phenethylamine class. (±)-4′-Methylmethcathinone [29–35] (Scheme 1) is a synthetic β-ketoamphetamine that is structurally related to cathinone, a psychoactive compound found in *Catha edulis (Khat)*. *Catha edulis* is a plant native to the Horn of Africa and the Arabian Peninsula whose leaves are chewed by natives whilst in a social environment. The consumption of *Catha edulis* has become an issue in the U.K. prompting several government reports into the social harms and legislation surrounding this material. [36, 37] (±)-4′-Methylmethcathinone has recently emerged in

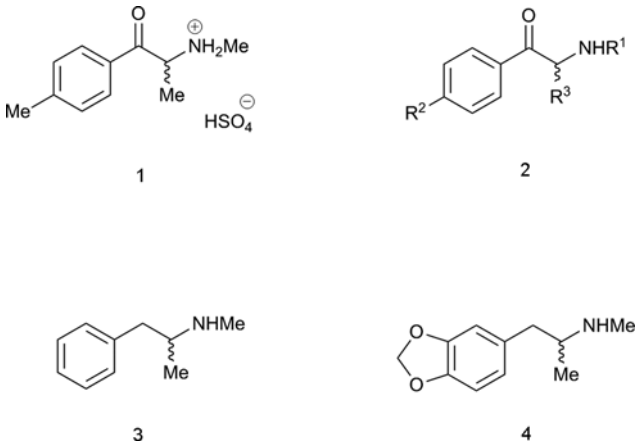

Scheme 1: Schematic of (±)-mephedrone hydrogen sulphate (**1**); general cathinone structure (**2**); methamphetamine (**3**); and MDMA (**4**).

drug seizures, as a "*legal high*" replacement for controlled stimulants, including methamphetamine and 3,4-Methylenedioxymethamphetamine (MDMA; Ecstasy) (Scheme 1). (±)-4′-Methylmethcathinone is now a substance controlled by legislation in the United Kingdom, Germany, Norway, Sweden, the Netherlands, Finland, Romania, Republic of Ireland, Denmark, Canada and Israel. These legislative changes have been introduced without an understanding of the solid-state structure of the pure substances and hence an understanding what impact the physicochemical properties has on the bioavaibility i.e. do different batches of street samples contain the same polymorph? If not, is the variaibility in polymorph a contributing factor to the variation in side-effects and instances of overdosing?

The aim of the present study is to characterise the novel salt, (±)-4′-methylmethcathinone hydrogen sulfate (4-MMC) with a view to understanding its polymorphic behaviour. In this study 4-MMC is subjected to both a ambient pressure solvent screen and compression study.

Experimental

Synthesis of (±)-4′-methylmethcathinone hydrogen sulfate (4-MMC)

The synthesis and full structural charaterisation of the title compound is detailed in the Supplementary Material.

Crystal Growth

5 mg (0.02 mmol) of the required 4-MMC was weighed accurately into 5 cm^{-3} vials before ~1 cm^{-3} of solvent was added. The solutions were heated to 313 K and stirred until all the material was dissolved before cooling to room temperature. The vials were stored and the solvent was allowed to evaporate. The colourless crystals were analysed using a range of techniques described below. Due to solubility issues a limited range of solvents of a variety of different properties were investigated (Table S-1).

High pressure

A Merrill-Bassett diamond anvil cell was equipped with 600 μm culet diamonds attached to tungsten carbide backing discs. A 300 μm hole was drilled in a preindented 200 μm thick tunsten foil to serve as the sample chamber. A piece of ruby was placed in the chamber so that the pressure could be measured *in-situ* using the Ruby fluorescence technique using a ThermoScientific DXR Raman microscope using a 532 nm laser [38].

A crystal of the compound of interest was added to the sample chamber and petroleum ether was used as a pressure transmitting medium [39]. X-ray diffraction data were collected at regular intervals.

Single crystal X-ray diffraction

The X-ray intensities of all the samples were measured on a Bruker-Nonius APEX II diffractometer using Mo*Kα* radiation. This diffractometer was upgraded during this study to a Bruker-Nonius DUO system utilising a Incoatec Microsource (0.71073 Å). The data collection and processing procedures for the high-pressure samples was carried out using the those outlined in Dawson et al. [40]. Integration was performed using SAINT implementing the dynamic masking procedure described in Dawson et al. The absorption correction was applied using programs SHADE [41] and SADABS [42].

The pressure dataset presented herein has used four separate crystals during the data collection; one at ambient pressure; one for collections at 0.5 and 1.97 GPa; one for data collections 0.88, 2.96 and 3.56 GPa; and one at 4.8 GPa. The high number of crystals for the high pressure datasets was due to overcompression during the first experiments (0.5 and 1.97 GPa) as well as to obtain a sufficiently good dataset in order to solve and refine a model for Phase III. A second crystal was loaded into the cell to bridge the pressure gaps in the first set of data. This negated any hysteresis effects that may have been present if data were collected on decompression. The orientation of this crystal gave a greater number of reflections however the number of independent reflections was reduced. Again, this crystal did not provide good enough data for structural solution. The fourth crystal was of higher quality and the structure of Phase III solved and refined against it. The number of independent reflections used in the structural refinement varied a little over the datasets and the completeness of the data remained constant at ~53% which is reasonable for a high-pressure study.

Phases I and III were solved by direct methods (SIR-92 [43]) and refined against F^2 using all data. Phase II was solved from the Phase I structure by separately grouping the methylmethcathonate cation and hydrogen sulfate anions to be rigid bodies and allowing the molecular positions to refine in CRYSTALS [44]. By this meth-

od the general molecular position and orientation were found before relaxing the rigid body constraint so that the individual atomic positions could be refined. Despite the low data completeness of the high-pressure phases, all non-H atoms were refined anisotropically for Phases I and II with the alkyl hydrogens placed and allowed to ride on their parent atoms. The data:parameter ratio is ~5 (with anisotropic atoms) and so it was felt that the refinement of thermal parameters was reasonable. 1,2 and 1,3 thermal similarity and vibrational restraints were used to ensure reasonable bahaviour. Due to the large number of atoms in Phase III the non-H atoms were refined isotropically. The ammonium hydrogen atoms and the hydroxyl hydrogen atoms were found on the difference map and restrained at an appropriate distance before allowing them to ride on the parent atom. Distance restraints were used in the refinements of all Phases. The distances used in the restraints were based on those calculated from the ambient pressure model. They were used in order that the molecules retained a sensible geometry given that the intramolecular bond lengths are not going to be affected by the pressures applied in this study. The crystal structure data for all datasets are found in Table 1.

Table 1: Experimental details for 4-MMC at various pressures

	SO4_293K	SO4_P1	SO4_P2	SO4_P3	SO4_P4	SO4_P5	SO4_P6
Crystal data							
Chemical formula	$C_{11}H_{16}NO \cdot HO_4S$	$C_{11}H_{16}NO \cdot HO_4S$	$C_{11}H_{16}NO \cdot HO_4S$	$C_{11}H_{16}NO \cdot HO_4S$	$C_{11}H_{16}NO \cdot HO_4S$	$C_{11}H_{16}NO \cdot HO_4S$	$C_{11}H_{16}NO \cdot HO_4S$
M_r	275.33	275.33	275.33	275.33	275.33	275.33	275.33
Crystal system, space group	Monoclinic, $P2_1/c$	Monoclinic, $P2_1/c$	Monoclinic, $P2_1/c$	Monoclinic, $P2_1/c$	Monoclinic, $P2_1/c$	Monoclinic, $P2_1/c$	Triclinic, $P\bar{1}$
Temperature (K)	293	293	293	293	293	293	293
Pressure (GPa)	Ambient	0.5	0.88	1.97	2.96	3.56	4.8
Phase	I	I	II	II	II	II	III
a, b, c (Å)	12.1067 (4), 8.7626 (2), 12.9731 (4)	12.1089 (19), 8.7603 (7), 12.9947 (8)	11.3005 (16), 8.9263 (7), 12.3704 (8)	11.150 (2), 8.8498 (8), 12.1965 (10)	11.056 (3), 8.8131 (10), 12.0501 (12)	10.978 (3), 8.976 (13), 11.9378(15)	10.956 (2), 14.0700 (15), 14.4090 (16)
α, β, γ (°)	90, 98.018 (2), 90	90, 98.040 (8), 90	90, 101.437 (9), 90	90, 101.104 (9), 90	90, 100.924 (12), 90	90, 100.726 (15), 90	76.151 (8), 79.001 (11), 80.006 (13)
V (Å^3)	1362.81 (7)	1364.9 (3)	1223.0 (2)	1180.9 (3)	1152.8 (3)	1132.8 (4)	2097.9 (5)
Z	4	4	4	4	4	4	8
Radiation type	Mo$K\alpha$	Mo$K\alpha$	Mo$K\alpha$	Mo$K\alpha$	Mo$K\alpha$	Mo$K\alpha$	Mo$K\alpha$
μ (mm^{-1})	0.25	0.25	0.28	0.29	0.30	0.30	0.33
Crystal size (mm)	0.25 × 0.18 × 0.15	0.15 × 0.10 × 0.10	0.20 × 0.20 × 0.05	0.15 × 0.10 × 0.10	0.20 × 0.20 × 0.05	0.20 × 0.20 × 0.05	0.10 × 0.10 × 0.05
Data collection							
Diffractometer	Bruker Kappa Apex2 diffractometer	Bruker Kappa Apex2 diffractometer	Bruker Kappa Apex2 diffractometer	Bruker Kappa Apex2 diffractometer	Bruker Kappa Apex2 diffractometer	Bruker Kappa Apex2 diffractometer	Bruker Kappa Apex2 diffractometer
Absorption correction	Multi-scan *SADABS* (Siemens, 1996)	Multi-scan *SADABS* (Siemens, 1996)	Multi-scan *SADABS* (Siemens, 1996)	Multi-scan *SADABS* (Siemens, 1996)	Multi-scan *SADABS* (Siemens, 1996)	Multi-scan *SADABS* (Siemens, 1996)	Multi-scan *SADABS* (Siemens, 1996)
T_{min}, T_{max}	0.91, 0.96	0.86, 0.98	0.79, 0.99	0.82, 0.97	0.86, 0.99	0.83, 0.99	0.92, 0.98
No. of measured, independent and observed [$I > 2.0\sigma(I)$] reflections	9514, 2781, 2477	2691, 929, 656	5205, 869, 599	4978, 857, 661	4245, 824, 623	4245, 824, 623	2175, 2175, 1575
R_{int}	0.017	0.050	0.077	0.063	0.073	0.073	0.078
θ_{max} (°)	26.4	23.3	23.3	23.3	23.4	23.5	23.3
Refinement							
$R[F^2 > 2\sigma(F^2)]$, $wR(F^2)$, S	0.041, 0.127, 0.91	0.048, 0.121, 1.01	0.049, 0.109, 1.02	0.059, 0.144, 1.03	0.069, 0.160, 1.02	0.069, 0.147, 1.10	0.085, 0.218, 1.00
No. of reflections	2771	922	863	851	818	818	2157
No. of parameters	163	163	163	163	163	163	289
No. of restraints	0	155	155	155	155	155	64
$\langle\Delta\rangle_{max}$, $\langle\Delta\rangle_{min}$ (e Å^{-3})	0.29, −0.37	0.34, −0.32	0.46, −0.50	0.40, −0.45	0.48, −0.52	0.49, −0.53	0.62, −0.60

Computer programs: Apex2 (Bruker AXS, 2006), SIR-92 (Altomare, 1994), *CRYSTALS* (Betteridge et al., 2003).

All crystal structures were visualised using the programs Mercury. Other structural analyses were carried out using PLATON [45] incorporated in the crystallographic suite WIN-GX [46]. Calculation of strain tensors was carried out using the program STRAIN [47] using the method described in R. M. Hazen and L. W. Finger [48]. Eigenvalues and vectors calculated using JACOBI routine [49]. Figures were produced using either Mercury [50] or Vesta [51] with further manipulation using GIMP 2.0 [52].

Cambridge Structural Database search

A search was conducted using two 1,4-dimethylbenzene fragments as a molecular search with no hydrogen atoms present. The Cambridge Structural Database (CSD) (version 5.34) was searched using Conquest version 1.15 [53]. Only organic, non-polymeric structures with 3D coordinates, no disorder, and no errors were searched. The centroids and planes of the phenyl rings were calculated and the distances between centroids and angle between planes retrieved with distance limits between 3.0 and 6.0 Å.

Two separate searches of the hydrogen bonding distances were conducted on a) $C_2N{-}H\cdots O{=}(S)$ and b) $SOH\cdots O{=}(S)$ moieties with a contact distances defined by the sum of the van der Waals radii. Only organic, non-polymeric structures with 3D coordinates, no disorder, no errors, and with an *R*-factor $\leqq 0.075$ were searched.

Results & discussion

Phase I

4-MMC was subjected to a solvent screen under ambient conditions before investigating the high pressure behaviour. During this solvent screen it became apparent that the hydrogen sulfate does not crystallise readily and a yellow glassy solid was formed from several crystallisation experiments; the yellow colour suggesting that decomposition occurs during recrystallisation. Crystals that were harvested within a relatively short time period did not show the discolouration. DSC and hot-stage microscopy analysis shows that the melting point of the hydrogen sulfate is relatively low (377 K) (Fig. S-2.6).

The crystal structure reveals that the sulfuric acid (H_2SO_4) has been singly deprotonated to hydrogen sulfate (HSO_4^-) such that there is only one cation and one

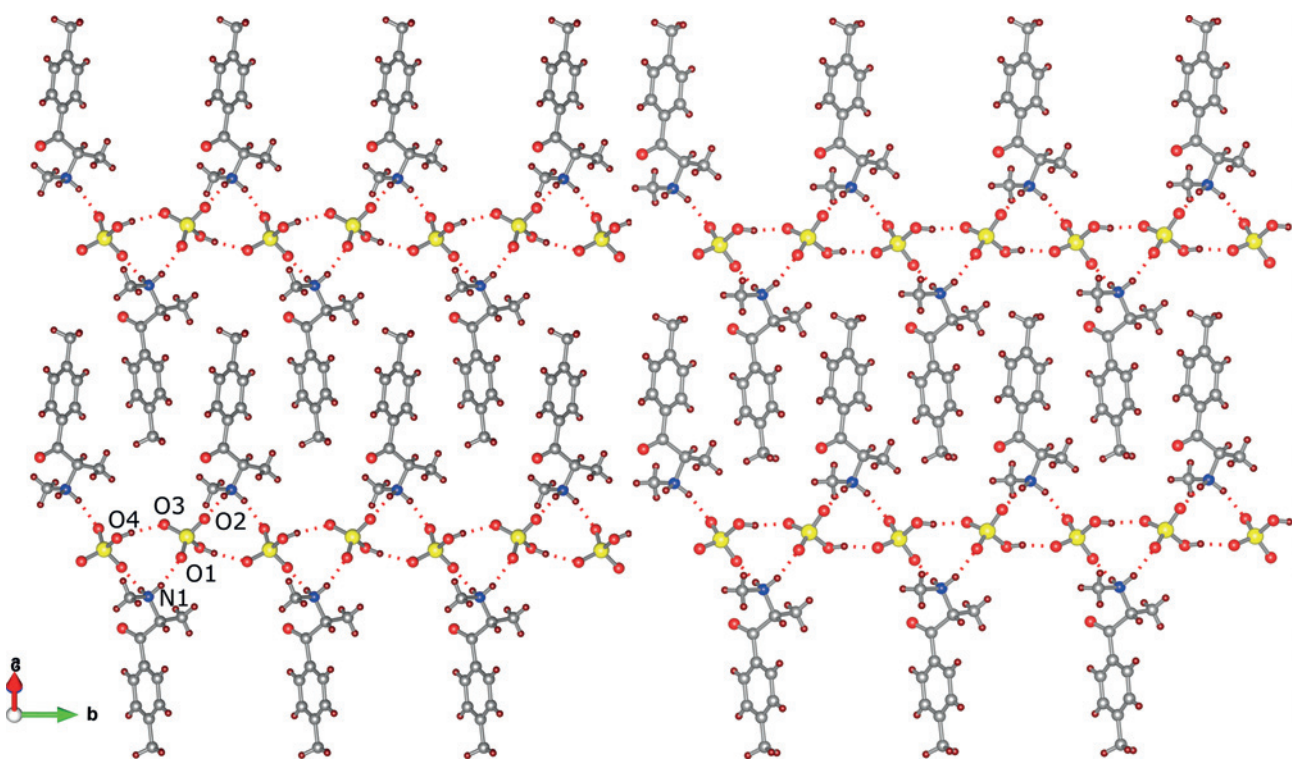

Fig. 1: Hydrogen bonded chains in compound 1 at 0.5 GPa (Left) and 0.88 GPa (right). Form II shows a slight increase in the intercalation of the neighbouring chains that reside in the same plane.

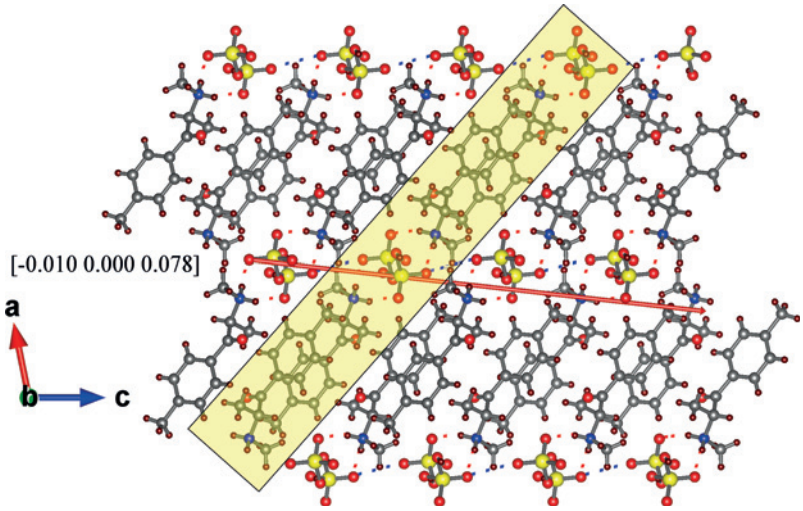

Fig. 2: View along the *b*-axis at 0.88 GPa. The layer from Fig. 1 is highlighted by the yellow rectangle. Also shown is the direction of greatest compression in Phase II i.e. approximately perpendicular to the layers.

anion in the asymmetric unit. Hydrogen bonded chains are formed by the interaction of the cation with the anion along the *b*-axis (N12 · · · O1 2.812(2) Å; N12 · · · O2 2.882(2) Å). Further hydrogen bonds are present from the HSO_4^- to a symmetrically equivalent molecule which completes the chain and a $R_3^3(10)$ ring motif (O4 · · · O3 2.641(2) Å) (Fig. 1). In order to make more sense of the high-pressure structure it is convenient to describe the structure through a 'layer' concept whereby the separate chains link through interactions between phenyl groups to form an extended layer using an edge-to-face arrangement (Fig. 2). There are no hydrogen bonds formed between the layers and the only contacts are between the oxygen atoms of the sulfate group and CH group of the cation. The first two contacts are between H101/H61 and O2 in a bifurcated bond with the layer above whilst there are two separate contacts between H13 · · · O4 and H133 · · · O3 to the layer below.

Compression of Phase I and the phase transformation to Phase II

As pressure is applied to a crystal of 4-MMC, two of the unit cell parameters actually increase (*a*- and *c*-axes) whilst the third shows very small decrease. The change in structure is smooth until the phase transformation. Between 0.5–0.9 GPa there is subtle phase transformation to a new phase, designated Phase II. The unit cell parameters (Fig. 3), and the discontinuities along each axis, support the conclusion of a transition to a new phase; the unit cell contracts by 10.4% over the phase transition (c.f. 3.4% change from 0.88 GPa to 1.97 GPa). The new structure retains the same space group ($P2_1/c$) and number of independent molecules ($Z' = 1$). Full refinement details can be found in Table 1.

The three main hydrogen bonds that are used in the chains show a variation in their response to pressure.

Table 2: Non-covalent parameters for 4-MMC at various pressures. All distances are in Å and angles in °. The roman numerals represent symmetry operations that are required to visualise the acceptor atom. No roman numerals represent interactions between molecules in the same asymmetric unit.

Pressure Phase	Ambient I	0.5 I	0.88 II	1.97 II	2.96 II	3.56 II	4.8 III	4.8 III	4.8 III	4.8 III
N(12)–H(121) · · · O(2)	2.920(2)^{i}	2.923(6)^{i}	2.799(6)^{i}	2.774(6)^{i}	2.766(8)^{i}	2.742(8)^{i}	2.713(14)^{iv}	2.717(13)	2.782(17)^{vii}	2.755(18)^{ix}
N(12)–H(122) · · · O(1)	2.828(2)^{ii}	2.818(7)^{ii}	2.815(8)^{ii}	2.794(9)^{ii}	2.769(11)^{ii}	2.756(11)^{ii}	2.75(2)^{v}	2.790(19)	2.779(19)	2.88(2)^{vii}
O(4)–H(411) · · · O(3)	2.641(2)^{iii}	2.641(6)^{iii}	2.575(6)^{iii}	2.539(7)^{iii}	2.538(9)^{iii}	2.533(9)^{iii}	2.514(14)^{vi}	2.486(12)	2.452(13)^{viii}	2.543(12)^{vii}
C5C8C10N12	159.68(16)	160.5(5)	156.2(5)	154.7(6)	153.5(8)	153.7(7)	112.5(15)	162.6(12)	−161.5(13)	123.8(14)
<O2–O4 · · · O3–O1	−88.18(7)	−88.2(2)	−94.5(2)	−93.7(3)	−94.0(4)	−93.79(6)	mol1-mol4 −124.8(7)	mol4-mol2 111.0(7)	mol2-mol3 86.1(7)	mol3-mol1 −142.6(6)
< between L.S. planes of phenyl groups	64.6(6)	64.23(16)	72.04(16)	73.71(19)	74.8(2)	75.0(3)	mol1-mol2 72.4(5)	mol2-mol3 84.6(5)	mol3-mol4 60.5(4)	mol4-mol1 74.4(4)

Symmetry operators: (i) $x, {}^{3}/_{2} - y, -{}^{1}/_{2} + z$; (ii) $-x, 1 - y, 1 - z$; (iii) $-x, 1/_{2} + y, {}^{3}/_{2} - z$; (iv) $1 - x, 1 - y, 2 - z$; (iv) $1 - x, 1 - y, 2 - z$; (v) $-1 + x, 1 + y, z$; (vi) $x, 1 + y, z$; (vii) $2 - x, 1 - y, 1 - z$; (viii) $2 - x, 1 - y, 2 - z$; (ix) $2 - x, -y, 1 - z$.

The hydrogen bonds lengths for NH(121)···O2 and OH(411)···O3 show a significant decrease over the transition whilst the NH(122)···O1 bond shows a gradual change with pressure despite the increase in the *b*-axis direction (Table 2). A significant change that has impacted on these hydrogen bonds is the rotation of the HSO_4^- units with respect to each other along the chain. The torsional angle, O2···O4···O3···O1 exhibits a sharp change from approximately −88.2(2)° in Phase I (0.5 GPa) to −94.5(2)° in Phase II (at 0.88 GPa) (Fig. 4).

Compression of Phase II and the phase transformation to Phase III

The compression of Phase II is anisotropic with the *c*-axis showing the greatest compression (3.5%) followed by the *a*-axis (2.9%) and then *b*-axis (1.4%). The unit cell parameters were used to determine the principal directions of strain during compression. The strongest compression is along the [−0.010 0.000 0.078] direction which is perpendicular to the layers of the structure (Fig. 2). At 0.88 GPa, these layers are separated by approximately 4.823 Å and are compressed to 4.578 Å at 3.56 GPa. The second greatest compression is observed within the layers perpendicular to the hydrogen bonds and pushes neighbouring chains together. It is not surprising that these two directions show the greatest change as the intermolecular interactions are limited to van der Waals contacts between molecules. During the compression the OH(411)···O3 has reached its minimum by 1.97 GPa (2.575–2.533 Å) and does not varying significantly to 3.56 GPa. Conversely, the other two hydrogen bonds NH(121)···O2 and NH(122)···O2 compress continuously to 3.56 GPa both reducing by 2% over the pressure range.

At approximately 4.8 GPa the crystal structure undergoes a phase transition to a new phase, denoted Phase III and fortunately, this transition is another single-crystal-to-single-crystal phase transformation therefore single-crystal diffraction data could be used to elucidate the structure of the new phase; the crystal data can be found in Table 1. The unit cell parameters of Phase II are related to those of Phase III via the matrix (−1 0 0 0 −1 1 0 1 1).

The structure is observed to be triclinic $P\bar{1}$ with four molecules in the asymmetric unit. The packing of the molecules in phase III is similar to the packing in the other two phases however there is further reorientation of the $HSO4^-$ groups with respect to one another (Fig. 4) but there are also significant changes to the molecular geometries of the cations particularly in relation to the tail group (C5–C8–C10–N12); both these changes cause a break and lowering of the symmetry (Fig. 5). A consequence of the reduction in symmetry is that there are

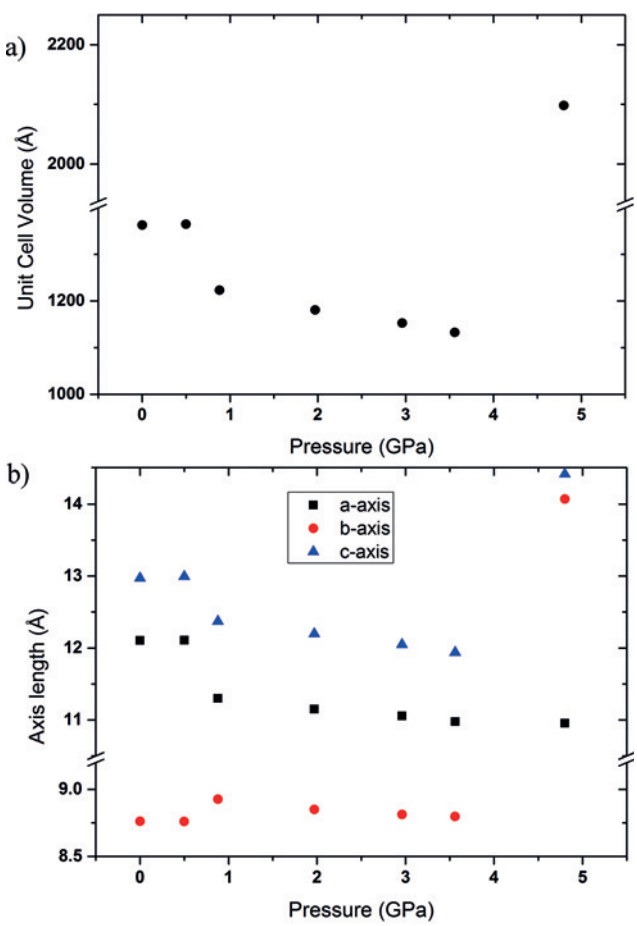

Fig. 3: (a) Unit cell volume; and (b) unit cell parameters of 4-MMC with increasing pressure. The discontinuities after 0.5 and 3.5 GPa show the phase transitions.

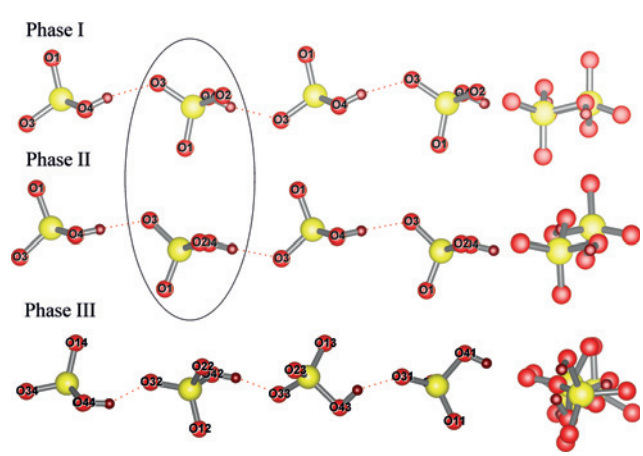

Fig. 4: The HSO_4^- chains in each of the three phases. The subtle rotation of the HSO_4^- groups between Phases I and II is highlighted. On the right-hand side is a projection along the hydrogen-bonded chains.

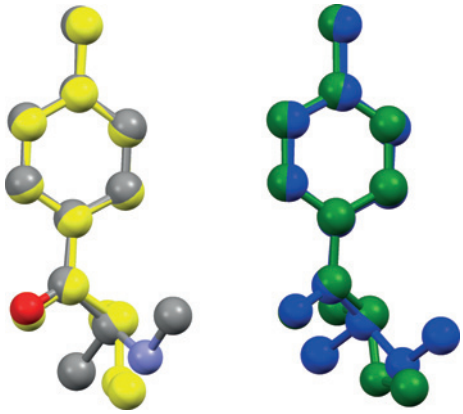

Fig. 5: The overlay of molecules in phase III showing the changes in torsional angle (N12-C10-C8-C5). For clarity molecules 1 and 2 are shown on the left and molecules 3 and 4 on the right.

now four independent hydrogen bonds between the HSO_4^- groups (2.452–2.543 Å). The large variation in the lengths of these bonds can be accounted for by the packing of the phenyl groups of the cation of neighbouring chains. The shorter O···O bonds are observed where the phenyl groups of neighbouring chains are more perpendicular to the Least Squares plane of the layer. The angle of the phenyl groups of molecules 1, 2, 3 and 4 to the Least Squares plane of the layer are 40.26°, 32.25°, 52.89°, and 66.77°, respectively. In relation to the hydrogen bonding, molecules 1 and 2, whose phenyl group are more parallel, are positioned in line with the O44···O32 (2.543(12) Å) and O41···O34 (2.514(14) Å) hydrogen bonds whilst molecules 3 and 4 (more perpendicular) are in line with the O43···O31 (2.452(13) Å) and O42···O33 (2.486(12) Å) hydrogen bonds. In this structure the packing of the molecules taking precedent over lengths of hydrogen bonding which is also observed in many other systems at high pressure [22–24, 54, 55].

Both of the phase transitions are reversible which has been observed via Raman spectroscopy. Fig. S-2.7 shows the Raman spectrum for 4-MMC at 0.5 GPa as well as a plot of the carbonyl stretch that shows the greatest change over the compression [56]. From this graph one can observe that the carbonyl stretch for the final decompressed sample returns to a value close to the ambient pressure form indicating that the phase transformations were reversible.

Comparison with the Cambridge Structural Database

The hydrogen bonding in all these phases is observed to be well within the limits of the data mined from the CSD

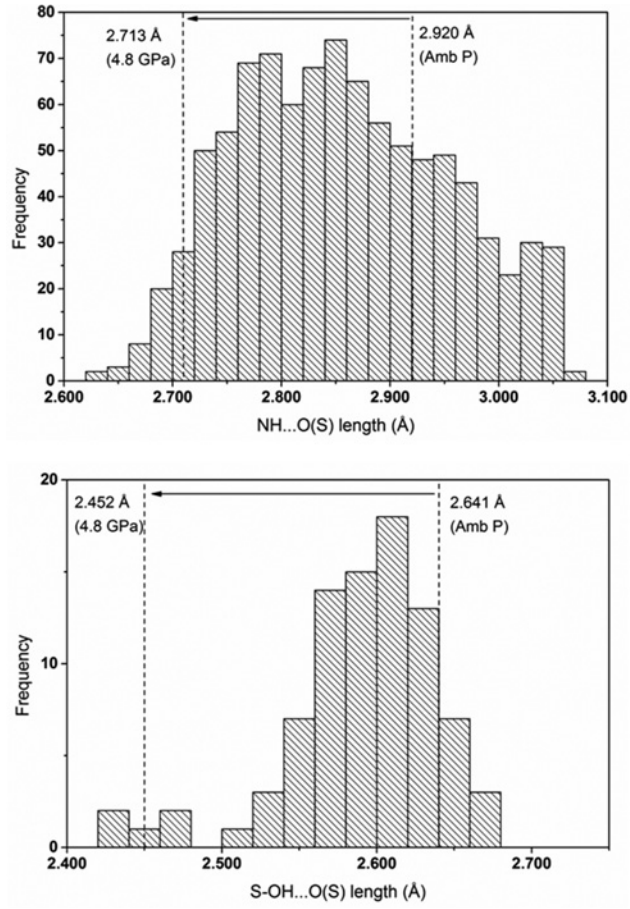

Fig. 6: Distributions of hydrogen bond lengths in the CSD. The dotted lines represent the distances observed in 4-MMC on compression.

[53]. Figure 6 shows the distribution of both types of hydrogen bond present within the structures of 4-MMC and where the ambient pressure phases lie within them. At

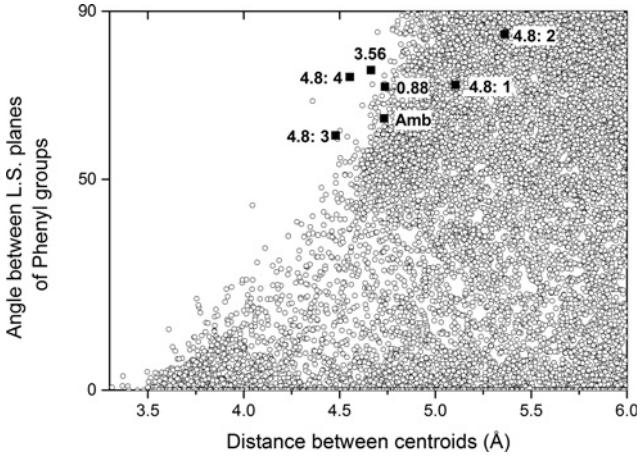

Fig. 7: Scatterplot of distance between centroids of phenyl groups and the angle between the Least Squares plane of the phenyl groups. Open circles are data from CSD and filled squarea are observations from this work.

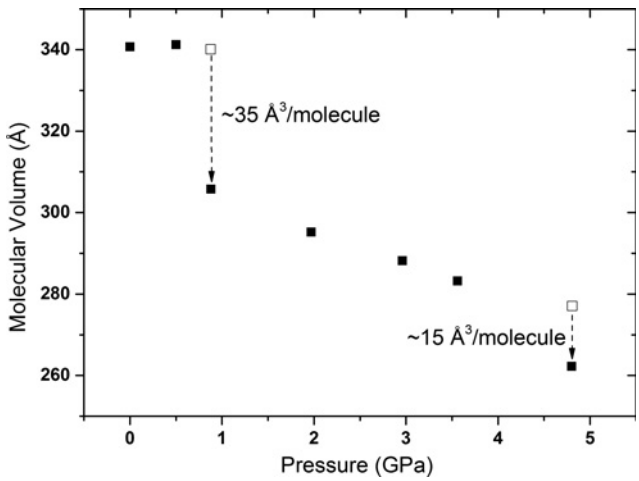

Fig. 8: Molecular volume vs. Pressure plot. The solid squares represent data collected in this study and the unfilled squares represent volumes for hypothetically compressed phases of I and II, respectively, to illustrate the significance of the pV term.

the phase boundary between Phases I and II, the hydrogen bond distances are observed to be longer than the minimum distance in the CSD (NH···O 2.923 & 2.818 Å cf. 2.62 Å; OH···O 2.641 Å cf. 2.42 Å). Previous work has suggested that upon reaching a minimum distance observed in the CSD a material will undergo a phase transition in order relieve the repulsion of the interactions [14, 57]. This is not observed in this structure therefore other factors must be dictating the change in phase. A significant portion of the structure relates to phenyl group interactions which have been summarised using two parameters; their inter-centroid distances and the interplanar angle between the phenyl groups (Fig. 7). It can be seen that our observation in Phase I is close to the limit of those observed in the CSD (4.733 Å, 64°) and over the transition this interaction shows little change (4.737 Å, 72°) except for the interplanar angle. This implies that this interaction is not particularly influential in terms of the phase transition which has been observed for similar interactions in salicylaldoxime [58]. Compression from Phase II–III shows a marked change in the interaction parameters. At 3.56 GPa (Phase II) the interaction has moved close to the limit observed in the CSD. Further

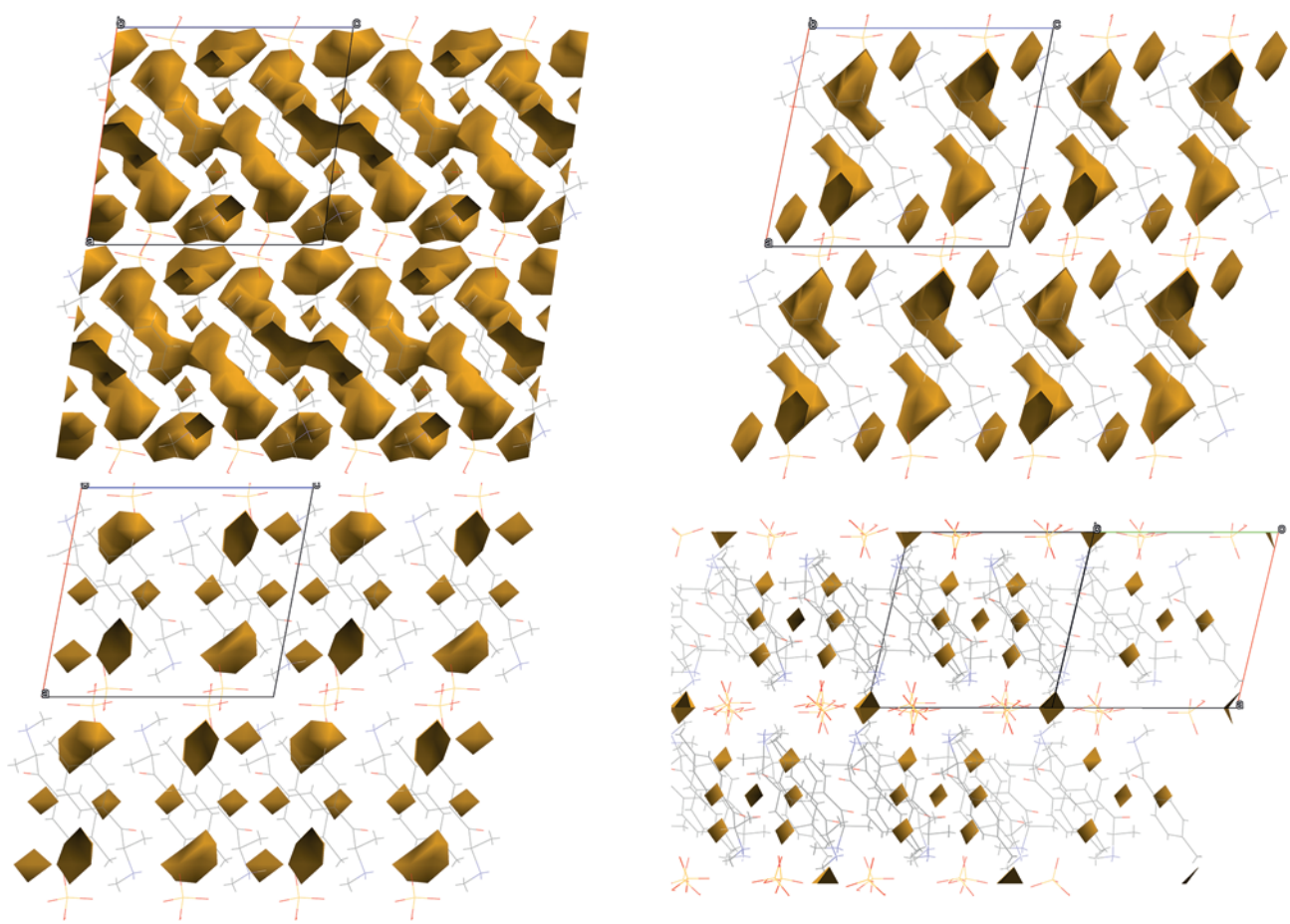

Fig. 9: Voids observed (and their total volume) at a) 0.5 GPa (94 Å³); b) 0.88 GPa (35 Å³); 3.56 GPa (17 Å³); and 4.8 GPa (14 Å³). The molecules have been set to wireframe so as not to obstruct the view of the voids. The probe distance was set at 0.4 Å and grid spacing of 1 Å.

compression invokes the phase transition so that there are now four symmetry inequivalent interactions, two of which move significantly into the bulk of the data points (5.104 Å, 72.44°; 5.362, 84.54) whilst the other two interactions move further into a physical space that is not observed in the CSD (4.479 Å, 60.47°; 4.554 Å, 74.35°). This latter observation suggests that there is a repulsive force that is alleviated by the change in phase which is able to stabilise the other two non-ideal interactions. Further theoretical calculations such as PIXEL method would be required to answer this question conclusively.

One significant change is the molecular volume (~35 $Å^3$ $molecule^{-1}$ for Phase I–II; 15 $Å^3$ $molecule^{-1}$ for Phase II–III) which leads to the conclusion that the reduction in volume is the driving force for the phase transitions rather than relieving repulsive interactions (Fig. 8) [58]. In fact, if the Phase I is extrapolated to 0.88 GPa and Phase II is extrapolated to 4.8 GPa, the pV term in Gibbs Free energy calculation equates to approximately 18 $kJmol^{-1}$ and 43 $kJmol^{-1}$, respectively. In both these transitions these energy differences are substantial and will play a significant role determining the phase stability with pressure with the caveat that there are many other forces at play. One reason for the large changes in volume is the reduction in the voids present within the crystal. The compression of voids is a significant observation of organic materials at high pressure and can account for the large reduction in the volume [14, 15, 59]. Figure 9 shows the reduction of the number and size of the voids present in each of the phases. Between Phase I (0.5 GPa) and Phase II there is a reduction of the void space by 64% (94 $Å^3$ to 35 $Å^3$) whilst a more modest reduction of 18% from Phase II to Phase III (17 $Å^3$ to 14 $Å^3$). As a proportion of the total reduction in volume these changes represent 42% and 7% for I–II and IIIII phase transitions, respectively.

Conclusions

In this study we have shown that (±)-4′-methylmethcathinone hydrogen sulfate undergoes two phase transformations at high pressure (0.88 GPa and 4.8 GPa) whilst ambient pressure solvent screens have only highlighted one polymorph. Both of these phase transformations are single crystal-to-single crystal and are reversible on release of pressure. This observation is not desirable in the context of identifying possible polymorphs of illicit materials that may be observed under ambient conditions however this study does reinforce the concept that the reduction of void space and hence the pV term in the free energy calcualtion can be hugely influencial in phase transformations in a crystal structure.

Acknowledgements: We would like to thank Professor Simon Parsons (University of Edinburgh) for his helpful discussions and copies of SHADE and Eclipse. We would also like to thank the referees for their useful comments on the manuscript. We would like to thank the EPSRC for funding the Glasgow Centre for Physical Organic Chemistry from which the diffractometer was funded. We would also like to thank The Strathclyde Institute of Pharmacy and Biomedical Sciences for funding the diffractometer upgrade.

References

[1] Bernstein J.: Polymorphism – A Perspective. Crystal Growth & Design. **11**(3) (2011) 632–650.
[2] Bond A. D.; Boese, R.; Desiraju, G. R.: On the polymorphism of aspirin. Angewandte Chemie-International Edition. **46**(4) (2007) 615–617.
[3] Johnston A.; Bardin, J.; Johnston, B. F.; Fernandes, P.; Kennedy, A. R.; Price, S. L.; Florence, A. J.: Experimental and Predicted Crystal Energy Landscapes of Chlorothiazide. Crystal Growth & Design. **11**(2), 2011, 405–413.
[4] Florence A. J.; Johnston, A.; Price, S. L.; Nowell, H.; Kennedy, A. R.; Shankland, N.: An automated parallel crystallisation search for predicted crystal structures and packing motifs of carbamazepine. Journal of pharmaceutical sciences. **95**(9) (2006) 1918–1930.
[5] Iski E. V.; Johnston, B. F.; Florence, A. J.; Sykes, E. C. H.; Urquhart, A. J.: Carbamazepine on a carbamazepine monolayer forms unique 1D supramolecular assemblies. Chemical communications. **47**(34) (2011) 9627–9629.
[6] Iski E. V.; Johnston, B. F.; Florence, A. J.; Urquhart, A. J.; Sykes, E. C. H.: Surface-Mediated Two-Dimensional Growth of the Pharmaceutical Carbamazepine. Acs Nano. **4**(9) (2010) 5061–5068.
[7] Lopez-Mejias V.; Kampf, J. W.; Matzger, A. J. Polymer-Induced Heteronucleation of Tolfenamic Acid: Structural Investigation of a Pentamorph. Journal of the American Chemical Society. **131**(13) (2009) 4554–4555.
[8] Porter W. W.; Elie, S. C.; Matzger, A. J.: Polymorphism in carbamazepine cocrystals. Crystal Growth & Design. **8**(1) (2008) 14–16.
[9] Zakharov B. A.; Losev, E. A.; Kolesov, B. A.; Drebushchak, V. A.; Boldyreva, E. V.: Low-temperature phase transition in glycine-glutaric acid co-crystals studied by single-crystal X-ray diffraction, Raman spectroscopy and differential scanning calorimetry. Acta Crystallogr Sect B-Struct Sci. **68** (2012) 287–296.
[10] Ibberson R. M.; Parsons, S.; Allan, D. R.; Bell, A. M. T.: Polymorphism in cyclohexanol. Acta Crystallogr Sect B-Struct Sci. **64** (2008) 573–582.
[11] Torrisi A.; Leech, C. K.; Shankland, K.; David, W. I. F.; Ibberson, R. M.; Benet-Buchholz, J.; Boese, R.; Leslie, M.; Catlow, C. R. A.; Price, S. L.: Solid phases of cyclopentane: Combined

experimental and simulation study. J Phys Chem B. **112**(12) (2008) 3746–3758.

[12] Tumanov N. A.; Boldyreva, E. V.: X-ray diffraction and Raman study of DL-alanine at high pressure: revision of phase transitions. Acta Crystallogr Sect B-Struct Sci. **68** (2012) 412–423.

[13] Zakharov B. A.; Losev, E. A.; Boldyreva, E. V.: Polymorphism of "glycine-glutaric acid" co-crystals: the same phase at low temperatures and high pressures. Crystengcomm. **15**(9) (2013) 1693–1697.

[14] Moggach S. A.; Allan, D. R.; Morrison, C. A.; Parsons, S.; Sawyer, L. Effect of pressure on the crystal structure of l-serine-I and the crystal structure of l-serine-II at 5.4 GPa. Acta Crystallographica Section B. **61**(1) (2005) 58–68.

[15] Moggach S. A.; Allan, D. R.; Parsons, S.; Sawyer, L.; Warren, J. E.: The effect of pressure on the crystal structure of hexagonal l-cystine. Journal of Synchrotron Radiation. **12**(5) (2005) 598–607.

[16] Hunter S.; Davidson, A. J.; Morrison, C. A.; Pulham, C. R.; Richardson, P.; Farrow, M. J.; Marshall, W. G.; Lennie, A. R.; Gould, P. J.: Combined Experimental and Computational Hydrostatic Compression Study of Crystalline Ammonium Perchlorate. Journal of Physical Chemistry C. **115**(38) (2011) 18782–18788.

[17] Millar D. I. A.; Maynard-Casely, H. E.; Kleppe, A. K.; Marshall, W. G.; Pulham, C. R.; Cumming, A. S.: Putting the squeeze on energetic materials-structural characterisation of a high-pressure phase of CL-20. Crystengcomm. **12**(9) (2010) 2524–2527.

[18] Davidson A. J.; Oswald, I. D. H.; Francis, D. J.; Lennie, A. R.; Marshall, W. G.; Millar, D. I. A.; Pulham, C. R.; Warren, J. E.; Cumming, A. S.: Explosives under pressure – the crystal structure of gamma-RDX as determined by high-pressure X-ray and neutron diffraction. Crystengcomm. **10**(2) (2008) 162–165.

[19] Ciezak J. A.; Jenkins, T. A.; Liu, Z.; Hemley, R. J.: High-pressure vibrational spectroscopy of energetic materials: Hexahydro-1,3,5-trinitro-1,3,5-triazine. Journal of Physical Chemistry A. **111**(1), (2007) 59–63.

[20] Fabbiani F. P. A.; Dittrich, B.; Florence, A. J.; Gelbrich, T.; Hursthouse, M. B.; Kuhs, W. F.; Shankland, N.; Sowa, H.: Crystal structures with a challenge: high-pressure crystallisation of ciprofloxacin sodium salts and their recovery to ambient pressure. Crystengcomm. **11**(7) (2009) 1396–1406.

[21] Oswald I. D. H.; Chataigner, I.; Elphick, S.; Fabbiani, F. P. A.; Lennie, A. R.; Maddaluno, J.; Marshall, W. G.; Prior, T. J.; Pulham, C. R.; Smith, R. I.: Putting pressure on elusive polymorphs and solvates. Crystengcomm. **11**(2) (2009) 359–366.

[22] Allan D. R.; Clark, S. J.; Brugmans, M. J. P.; Ackland, G. J.; Vos, W. L.: Structure of crystalline methanol at high pressure. Physical Review B. **58**(18) (1998) R11809–R11812.

[23] Allan D. R.; Clark, S. J.; Dawson, A.; McGregor, P. A.; Parsons, S.: Pressure-induced polymorphism in phenol. Acta Crystallographica Section B. **58**(6) (2002) 1018–1024.

[24] Oswald I. D. H.; Crichton, W. A.: Structural similarities of 2-chlorophenol and 2-methylphenol. Crystengcomm. **11**(3) (2009) 463–469.

[25] Saouane S.; Norman, S. E.; Hardacre, C.; Fabbiani, F. P. A.: Pinning down the solid-state polymorphism of the ionic liquid bmim PF6. Chemical Science. **4**(3) (2013) 1270–1280.

[26] Zhu N.; Harrison, A.; Trudell, M.; Klein-Stevens, C.: QSAR and CoMFA Study of Cocaine Analogs: Crystal and Molecular Structure of (–)-Cocaine Hydrochloride and N-Methyl-3β-(p-Fluorophenyl)Tropane-2β-Carboxylic Acid Methyl Ester. Structural Chemistry. **10**(2) (1999) 91–103.

[27] Gabe E. J.; Barnes, W. H.: The crystal and molecular structure of l-cocaine hydrochloride. Acta Crystallographica. **16**(8) (1963) 796–801.

[28] Hillebrand J.; Olszewski, D.; Sedefov, R.: Legal Highs on the Internet. Substance Use & Misuse. **45**(3) (2010) 330–340.

[29] Schifano F.; Albanese, A.; Fergus, S.; Stair, J. L.; Deluca, P.; Corazza, O.; Davey, Z.; Corkery, J.; Siemann, H.; Scherbaum, N.; Farre, M.; Torrens, M.; Demetrovics, Z.; Ghodse, A. H.; Psychonaut Web, M.; Re, D. R. G.: Mephedrone (4-methylmethcathinone; 'meow meow'): chemical, pharmacological and clinical issues. Psychopharmacology. **214**(3) (2011) 593–602.

[30] Santali E. Y.; Cadogan, A.-K.; Daeid, N. N.; Savage, K. A.; Sutcliffe, O. B.: Synthesis, full chemical characterisation and development of validated methods for the quantification of (+/–)-4′-methylmethcathinone (mephedrone): A new "legal high". Journal of Pharmaceutical and Biomedical Analysis. **56**(2) (2011) 246–255.

[31] Kelly J. P.: Cathinone derivatives: A review of their chemistry, pharmacology and toxicology. Drug Testing and Analysis. **3**(7–8) (2011) 439–453.

[32] Gibbons S.; Zloh, M.: An analysis of the 'legal high' mephedrone. Bioorganic & Medicinal Chemistry Letters. **20**(14) (2010) 4135–4139.

[33] Deruiter J.; Hayes, L.; Valaer, A.; Clark, C. R.; Noggle, F. T.: methcathinone and designer analogs – synthesis, stereochemical analysis, and analytical properties. Journal of Chromatographic Science. **32**(12) (1994) 552–564.

[34] Dargan P. I.; Sedefov, R.; Gallegos, A.; Wood, D. M.: The pharmacology and toxicology of the synthetic cathinone mephedrone (4-methylmethcathinone). Drug Testing and Analysis. **3**(7–8) (2011) 454–463.

[35] Camilleri A.; Johnston, M. R.; Brennan, M.; Davis, S.; Caldicott, D. G. E.: Chemical analysis of four capsules containing the controlled substance analogues 4-methylmethcathinone, 2-fluoromethamphetamine, alpha-phthalimidopropiophenone and N-ethylcathinone. Forensic Science International. **197**(1–3) (2010) 59–66.

[36] Anderson D. M.; Carrier, N. C. M. Khat: Social harms and legislation – A literature review. In: Office H, ed. accessed 19th June 2013 ed: U.K. Government; 2011.

[37] Mathewson H.; James, K.; Schifano, F.; Sumnall, H.; Wing, A.; Anderson, D. Khat: A review of its potential harms to the individual and communities in the UK accessed 19th June 2013 ed: U.K. Government; 2013.

[38] Piermarini G. J.; Block, S.; Barnett, J. D.; Forman, R. A.: calibration of pressure-dependence of *R*1 ruby fluorescence line to 195 KBAR. J Appl Phys. **46**(6) (1975) 2774–2780.

[39] Tateiwa N.; Haga, Y.: Evaluations of pressure-transmitting media for cryogenic experiments with diamond anvil cell. Review of Scientific Instruments. **80**(12) (2009).

[40] Dawson A.; Allan, D. R.; Parsons, S.; Ruf, M.: Use of a CCD diffractometer in crystal structure determinations at high pressure. Journal of Applied Crystallography. **37**(3) (2004) 410–416.

[41] Parsons S.: SHADE. University of Edinburgh. 2004.

[42] Sheldrick G. M.: SADABS. University of Gottingen, Germany, Bruker AXS Madison, Wisconsin, USA. 2001.

[43] Altomare A.; Cascarano, G.; Giacovazzo, C.; Guagliardi, A.; Burla, M. C.; Polidori, G.; Camalli, M.: SIR92 – a program for auto-

matic solution of crystal structures by direct methods. Journal of Applied Crystallography. **27**(3) (1994) 435.
[44] Betteridge P. W.; Carruthers, J. R.; Cooper, R. I.; Prout, K.; Watkin, D. J.: Crystals version 12: software for guided crystal structure analysis. Journal of Applied Crystallography. **36**(6) (2003) 1487.
[45] Spek A.: Single-crystal structure validation with the program PLATON. Journal of Applied Crystallography. **36**(1) (2003) 7–13.
[46] Farrugia L.: WinGX suite for small-molecule single-crystal crystallography. Journal of Applied Crystallography. **32**(4) (1999) 837–838.
[47] Parsons S.: Strain. University of Edinburgh. (2003).
[48] Hazen R. M.; Finger, L. W.: Comparative Crystal Chemistry. Chichester: John Wiley & Sons (1982).
[49] Press W. H.; Teukolsky, S. A.; Vetterling, W. T.; Flannery, B. P.: Numerical Receipes in Fortran. Second Edition ed. Cambridge, England: Cambridge University Press (1992).
[50] Macrae C. F.; Bruno, I. J.; Chisholm, J. A.; Edgington, P. R.; McCabe, P.; Pidcock, E.; Rodriguez-Monge, L.; Taylor, R.; van de Streek, J.; Wood, P. A.: Mercury CSD 2.0 – new features for the visualization and investigation of crystal structures. Journal of Applied Crystallography. **41**(2) (2008) 466–470.
[51] Momma K.; Izumi, F.: VESTA 3 for three-dimensional visualization of crystal, volumetric and morphology data. Journal of Applied Crystallography. **44**(6) (2011) 1272–1276.
[52] Mattis P. K. S.: GNU Image Manipulation Program (wwwgimporg), Copyright ©. 2002, 2003, 2004, 2005, 2006, 2007, 2008, 2009, 2010.
[53] Allen F.: The Cambridge Structural Database: a quarter of a million crystal structures and rising. Acta Crystallographica Section B. **58**(3 Part 1) (2002) 380–388.
[54] Oswald I. D. H.; Allan, D. R.; Day, G. M.; Motherwell, W. D. S.; Parsons, S.: Realizing predicted crystal structures at extreme conditions: The low-temperature and high-pressure crystal structures of 2-chlorophenol and 4-fluorophenol. Crystal Growth & Design. **5**(3) (2005) 1055–1071.
[55] Seryotkin Y. V.; Drebushchak, T. N.; Boldyreva, E. V.: A high-pressure polymorph of chlorpropamide formed on hydrostatic compression of the [alpha]-form in saturated ethanol solution. Acta Crystallographica Section B. **69**(1) (2013) 77–85.
[56] Stewart S. P.; Bell, S. E. J.; Fletcher, N. C.; Bouazzaoui, S.; Ho, Y. C.; Speers, S. J.; Peters, K. L.: Raman spectroscopy for forensic examination of β-ketophenethylamine "legal highs": Reference and seized samples of cathinone derivatives. Analytica Chimica Acta. **711**(0) (2012) 1–6.
[57] Wood P. A.; McKinnon, J. J.; Parsons, S.; Pidcock, E.; Spackman, M. A.: Analysis of the compression of molecular crystal structures using Hirshfeld surfaces. CrystEngComm. **10**(4) (2008) 368–376.
[58] Wood P. A.; Forgan, R. S.; Henderson, D.; Parsons, S.; Pidcock, E.; Tasker, P. A.; Warren, J. E.: Effect of pressure on the crystal structure of salicylaldoxime-I, and the structure of salicylaldoxime-II at 5.93 GPa. Acta Crystallographica Section B. **62**(6) (2006) 1099–1111.
[59] Johnstone R. D. L.; Lennie, A. R.; Parsons, S.; Pidcock, E.; Warren, J. E.: Comparison of the effects of pressure on three layered hydrates: a partially successful attempt to predict a high-pressure phase transition. Acta Crystallogr Sect B-Struct Sci. **65** (2009) 731–748.

Received April 4, 2013; accepted June 26, 2013
Published online February 5, 2014